# Particle on a Rod: Surface-Tethered Catalyst on CdS Nanorods for Enzymatically Active Nicotinamide Cofactor Generation

*Lihini Jayasinghe[1], Jiaxi Wei[1], Jinhyun Kim[1,2], Elizabeth Lineberry[1], Peidong Yang[1,3,4,5*]*

[1] Department of Chemistry, University of California, Berkeley, Berkeley, CA 94720, USA.

[2] Department of Chemical and Biomolecular Engineering, University of California, Berkeley, Berkeley, CA 94720, USA

[3] Department of Materials Science and Engineering, University of California, Berkeley, Berkeley, CA 94720, USA.

[4] Materials and Chemical Sciences Division, Lawrence Berkeley National Laboratory, Berkeley, CA 94720, USA.

[5] Kavli Energy Nano Science Institute, Berkeley, CA 94720, USA.

KEYWORDS: CdS Nanorods, Photocatalysis, Charge transfer, Redox cofactors

*p_yang@berkeley.edu

ABSTRACT

The photochemical generation of nicotinamide cofactor 1,4-NADH, facilitated by inorganic photosensitizers, emerges as a promising model system for investigating charge transfer phenomena at the interface of semiconductors and bacteria, with implications for enhancing Photosynthetic Biohybrid systems (PBSs). However, extant semiconductor nanocrystal model systems suffer from achieving optimal conversion efficiency under visible light. This study investigates quasi-one-dimensional CdS nanorods as superior light absorbers, surface modified with catalyst Cp*Rh(4,4'-COOH-bpy)$Cl_2$ to produce enzymatically active NADH. This model subsystem facilitates easy product isolation and achieves a turnover frequency (TOF) of 175 $h^{-1}$, one of the highest efficiencies reported for inorganic photosensitizer-based nicotinamide cofactor generation. Charge transfer kinetics, fundamental for catalytic solar energy conversion, range from $10^6$ to $10^8$ $s^{-1}$ for this system highlighting the superior electron transfer capabilities of NRs. This model ensures efficient cofactor production and offers critical insights into advancing systems that mimic natural photosynthesis for sustainable solar-to-chemical synthesis.

Photosynthetic biohybrid systems (PBSs) combine the light-harvesting properties of inorganic semiconductors with biological machinery to enhance natural photosynthesis for sustainable solar-to-chemical synthesis.[1] Our model PBS employs the acetogenic bacterium *Moorella thermoacetica* integrated with biologically precipitated cadmium sulfide (CdS) nanoparticles to convert $CO_2$ to acetate under simulated sunlight.[1–3] Understanding the interface between inorganic and biological components, particularly the Wood-Ljungdahl Pathway (WLP) in acetogenic bacteria, which mediates $CO_2$ reduction to acetyl coenzyme A, is crucial. Proposed mechanisms for this charge transfer include indirect electron transfer via soluble redox mediators such as 1,4-dihydro nicotinamide adenine dinucleotide (1,4-NADH) or ferredoxin.[4] This study begins to

explore the biotic-abiotic interfaces PBSs by elucidating the charge transfer mechanism in a simplified subsystem between the photosensitizer, CdS and the WLP-participating cellular component 1,4-NADH, which is essential for over 80% of redox enzymes,[5–7] leading us to the fundamental revelation of whether CdS can be photoactivated to regenerate the redox component. NADH has been generated through enzymatic,[8,9] chemical,[10] electrochemical,[11,12] and photochemical,[13] approaches. While enzymatic methods are efficient, they face instability and high costs[14]. Chemical methods may introduce contaminants, and electrochemical methods, despite utilizing clean energy, limit optical probing. In contrast, photochemical methods harness solar energy but require enhancements in efficiency. [15–17] This study presents a novel approach aimed at addressing these limitations associated with traditional photoactivation methods.

Recently, Cd chalcogenide-based nanomaterials have shown promising charge transfer capabilities to biological species mainly due to the conduction band edge alignment with biological redox potentials.[18,19] However, little work has been done on nicotinamide cofactor generation with these nanomaterials. Existing findings suggest that quantum dots (QDs) have potential for in situ photochemical generation of 1,4-NADH under visible light.[18] Looking further Cd-chalcogenide nanorods (NRs) with quasi-one-dimensional geometry exhibit unique anisotropic features, such as directional light absorption and emission, and significant, tunable extinction coefficients.[20,21] Compared to QDs, NRs have significantly stronger absorption per volume and superior electron transfer capabilities. Their high surface-to-volume ratios position surface-adsorbed species near photoexcited carriers, and a single NR can support many attached charge acceptors.[20,22] Considering these factors, we propose NRs as superior candidates for NADH generation.

The reduction of $NAD^+$ is restricted by its dependence on the enzymatically active form 1,4-NADH. However, the recently reported $[Cp^*Rh(bpy)(H_2O)]^{2+}$ ($Cp^*=C_5Me_5$, bpy = 2,2'-

bipyridine), referred here to as M, as a catalyst for NADH generation, is capable of high selectivity.[23] In combination with the superior light absorbing properties of quasi-1D Cd-chalcogenides, we modified M, the parent compound, with carboxylic acid moieties as anchoring groups based on an approach for attachment of Ru(II) tris-bipyridyl complexes to the surfaces of CdSe QDs.[24] This surface-tethering approach of the catalyst onto the photosensitizer allows for the distinct isolation of enzymatically active NADH, providing a more controlled pathway for further investigation involving charge transfer.

Overall, the primary design principles for our model photosensitizer-catalyst system encompassed several key factors: (i) use of a previously unexplored class of nanomaterials in nicotinamide cofactor generation with superior optical and catalytic properties, (ii) the potential for surface modification to emulate a heterolytic catalyst, thereby improving product isolation, and (iii) feasible redox energy alignments that would allow electron transfer from the photoexcited nanoparticle to facilitate 1,4-NADH generation.

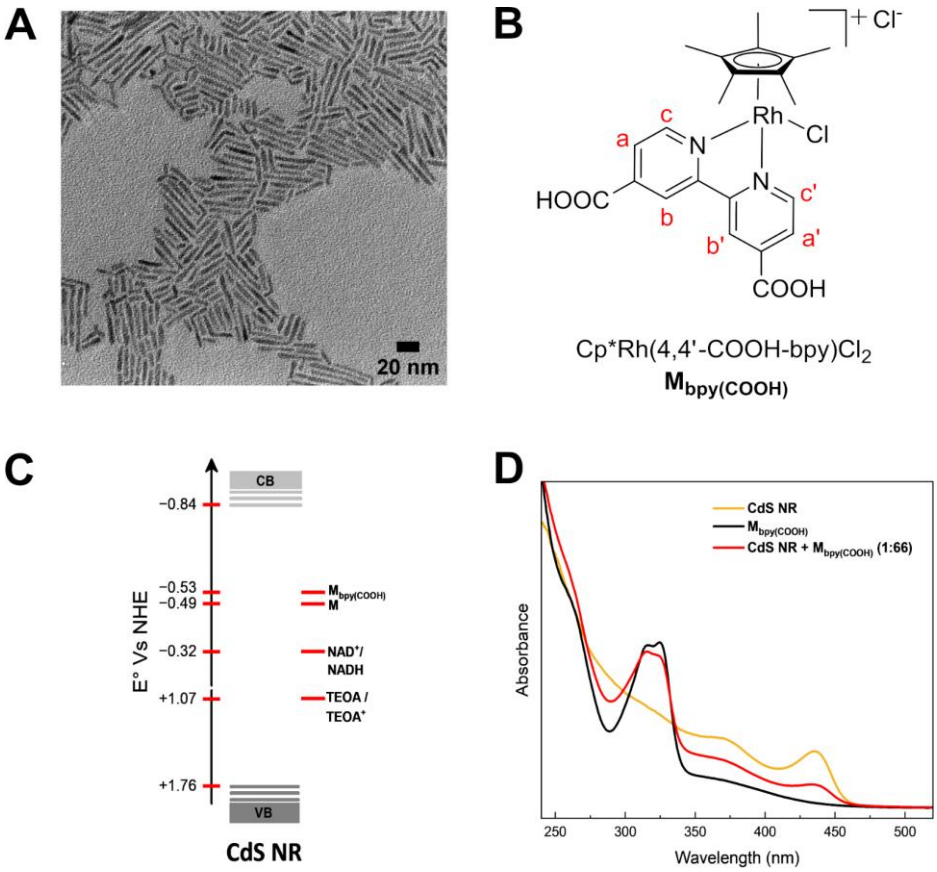


**Figure 1.** (A) TEM image of synthesized CdS NRs. (B) Chemical structure of the catalyst Cp*Rh(4,4'-COOH-bpy)$Cl_2$. (C) Energy level diagram showing the band edge of CdS NRs and redox potentials of M ($[Cp^*Rh(bpy)(H_2O)]^{2+}$), $M_{bpy(COOH)}$, $NAD^+$/NADH and electron donor TEOA. (D) UV-visible spectra of CdS NRs, $M_{bpy(COOH)}$, and the spectrum of surface-tethered CdS NRs after precipitation with anti-solvent and redissolving in methanol.

CdS NRs were synthesized following a well-established colloidal hot injection synthesis[25] (Refer to Supplementary Methods). Transmission electron microscopic (TEM) measurements showed highly monodispersed NRs (Figure 1A), ~24 nm in length and 4 nm in width obtained from the analysis of 200 particles (Figure S2). The estimated value for the molar extinction coefficient of

the CdS NRs was 6.3 x $10^6$ $M^{-1}$ $cm^{-1}$ at $\varepsilon_{350}$ (for calculation details refer SI). In the next step, the NRs were ligand-exchanged with 3-mercaptopropionic acid (3-MPA). The parent catalyst, M, was derivatized by addition of carboxylate functional group at the 4,4' meta positions on the bipyridine moiety following an established method of synthesis.[26] This modified catalyst is denoted as $M_{bpy(COOH)}$ (Figure 1B) throughout this communication. The energy level diagram in Figure 1C illustrates the redox potentials of the catalysts M and $M_{bpy(COOH)}$, the nicotinamide cofactors, conduction band minimum of CdS NRs determined by electrochemistry measurements (Figures S3A and S4) with a band gap of 2.60 eV measured using the Tauc plot (Figure S3B). Triethanolamine (TEOA) serves as the sacrificial electron donor for the regeneration of the CdS ground state. Through the alignment of energy levels, we verify the thermodynamic favorability of electron transfer from photoexcited CdS NRs to $M_{bpy(COOH)}$. This, coupled with the lower redox potential of the $NAD^+$/NADH redox couple, establishes the overall energetic feasibility of the reaction system. The selection of $M_{bpy(COOH)}$ thus integrates both structural insight and a consideration of redox properties with respect to band alignment.

The spectral characteristics of $M_{bpy(COOH)}$ were characterized by a maximum absorbance at 325 nm which could be attributed to metal-to-ligand charge transfer and used to determine the actual ratio of $M_{bpy(COOH)}$ to CdS in the modified NRs following a previously established procedure[27] (Figure S5; details in SI Methods). The molar extinction coefficient of the catalyst was determined based on this absorbance, yielding a value of 1.9x$10^5$ $M^{-1}$ $cm^{-1}$ (Figure S6). The CdS NR spectrum (Figure 1D) exhibits four well-defined absorption bands, with the lowest excitonic energy transition occurring at 435 nm. Upon attachment (discussed in detail later), the NRs and catalyst display no significant changes except a small change in peak height ratio at the maximum absorbance, as evidenced by their absorption spectra illustrated in Figure 1D. The highly

morphology-sensitive excitonic transitions of the NRs at 310, 370, and 435 nm remain unchanged, allowing us to optically confirm that $M_{bpy(COOH)}$ was not chemically modified, similar in observation to previous work involving the attachment of molecular catalysts onto the surface of CdS NRs.[27,28]

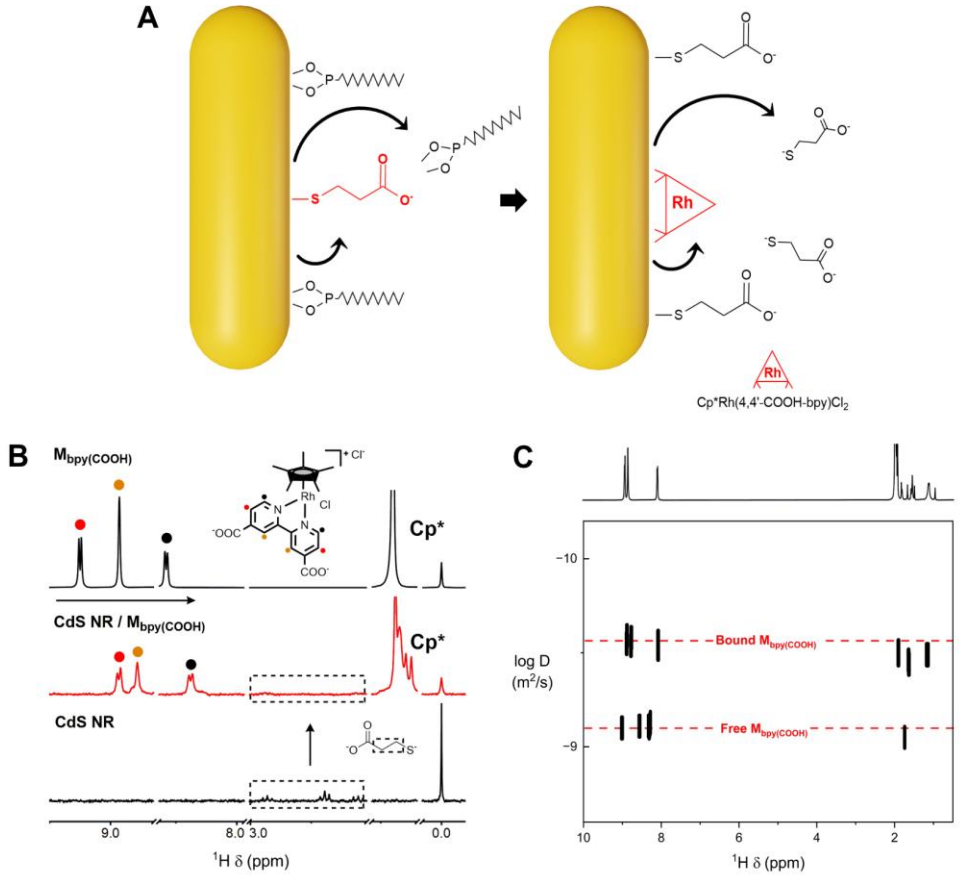


**Figure 2.** (A) Schematic of the key transformations that takes place on the surface of the CdS during surface coordination of $M_{bpy(COOH)}$ (B) $^{1}$H-NMR spectra of $M_{bpy(COOH)}$, CdS NRs and the surface modified CdS NRs that highlights line broadening and peak shifting due to surface attachment of catalyst. (C) 2D DOSY NMR spectra of a suspension of CdS NRs (138 μM) dissolved in deuterated methanol after surface treatment and precipitation.

Figure 2A illustrates the two-step process for the coordination of $M_{bpy(COOH)}$ onto the CdS NRs. NRs initially functionalized with thiolate groups, undergo coordination with the catalyst by treating them with $M_{bpy(COOH)}$ in deionized water at pH 7.4 for a duration ranging from 3 to 8 hours. At this pH, the carboxylic acid groups in $M_{bpy(COOH)}$ remain deprotonated, given their p$K_a$ range of 3.3-3.98.[29] Subsequently, careful purification by methanol-induced precipitation and centrifugation is employed to remove any residual catalysts. The NR/catalyst system is then re-dispersed in deionized water or methanol for further analysis. The X-ray photoelectron spectroscopy (XPS) survey measurement in Figure S7 obtained after various cycles of purification to remove any residual catalyst indicates that the $M_{bpy(COOH)}$ species remains on NR surface.

We hypothesize that the $COO^-$ groups on the catalyst can establish coordination with the $Cd^{2+}$ surface either through attachment to unpassivated $Cd^{2+}$ or via coordinate bonding, involving the replacement of existing 3-MPA ligands as evidenced by the disappearance of the peaks belonging to native mercaptopropionic species in the range of 2.5-3.0 ppm seen in the $^1$H Nuclear Magnetic Resonance (NMR) spectra shown in Figure 2B. The effect of interaction between the CdS NRs and $M_{bpy(COOH)}$ can be further seen by line broadening in the $^1$H-NMR spectra, which is a well-established phenomenon in the field of colloidal nanocrystals for protons close to a bound ligand's binding group.[30–33] The $^1$H-NMR spectra in Figure 2B, obtained after careful purification by methanol-induced precipitation and centrifugation to remove excess unbound ligands, show NMR resonances predominantly from surface-bound species and not from free ligands. In addition, the upfield shifting phenomenon may arise from variations in carboxylic acid binding modes. It has been reported that upfield-shifting and broadening of peaks corresponding to carboxylic acid moieties suggest a strong interaction between acid groups and the nanoparticle surface and that the broadening is likely attributed to chemical shift heterogeneity arising from a distribution of sites

at the nanoparticle surface.[32] The binding orientation of these moieties and an in-depth analysis of the surface changes have not been explored in this study as the primary focus of this study lies in laying the groundwork for surface-tethered nanomaterials in aqueous systems for biological cofactor generation.

To gain additional information about the surface interaction, we utilized two-dimensional (2D) diffusion ordered spectroscopy (DOSY), where the resonances of the free and surface-bound ligands are distinguishable along the diffusion dimension.[34,35] (Refer SI for experimental details). In the DOSY spectrum in Figure 2C, two sets of resonances for $M_{bpy(COOH)}$ can be distinguished, with a diffusion coefficient of $3.30\times10^{-10}$ $m^2/s$ for the surface coordinated catalyst on the CdS NRs. This is a reduction of 34% compared to that for $M_{bpy(COOH)}$ freely in solution, indicating the presence of catalyst-attached NRs that diffuse slower.

Furthermore, photoluminescence (PL) measurements on CdS NRs treated with $M_{bpy(COOH)}$ revealed that this catalyst strongly quenches the NRs' PL. $M_{bpy\ (COOH)}$ is nonemissive and does not contribute PL to the spectra. Both the PL from the band edge and trap states, under 360 nm excitation, diminish (see Figure 3A), and this reduction becomes more significant with a higher concentration of catalyst molecules with respect to a constant molarity of CdS NRs. The observed quenching cannot be explained by Förster resonant energy transfer, given the small spectral overlap between CdS NR emission and $M_{bpy(COOH)}$ absorption.[27,28] In this context, a Stern–Volmer model was applied to interpret the quenching mechanism. The integrated band edge (430–490 nm) and trap state (490–700nm) PL spectra was obtained as a function of CdS NR and increasing amount of $M_{bpy(COOH).}$ The observed deviation from a linear form indicates that the traditional

model of quenching through collisions of two species in solution is not applicable to our system (Figures S9A and S9B).[36] Instead when $M_{bpy(COOH)}$ is assumed to form a monolayer on CdS NRs, demonstrated through a Langmuir adsorption isotherm (Figures S9C and S9D), the Langmuir fit is superior indicating that the quenching behavior is driven at least moderately by adsorption. This corroborates the notion of chemisorption of $M_{bpy(COOH)}$ on the surfaces of CdS NRs as demonstrated similarly in the past.[27,28] (For details refer SI).

Investigation of the charge-transfer properties at the interface between the CdS NR and $M_{bpy(COOH)}$ was done using time resolved PL (TRPL). TRPL is a powerful technique that offers valuable insights into charge-carrier recombination and interfacial charge-transfer dynamics. It works by observing the decay trace of PL

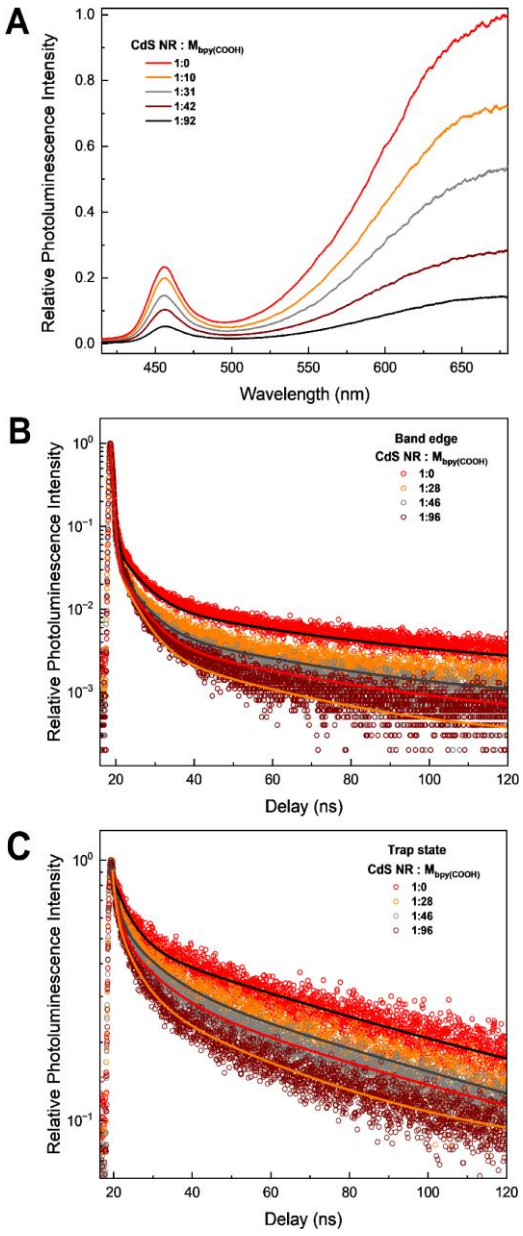


**Figure 3.** (A) PL quenching of CdS NRs at band edge and trap state with increasing coverage of $M_{bpy(COOH)}$ per CdS NR ($\lambda_{ex}$ = 360 nm). (B) (C) Band edge and trap state PL decay plots for CdS NRs coordinated to catalyst, respectively.

from the specific component being studied.[37–39] The observed decrease in CdS lifetime both at band edge and trap state with increasing $M_{bpy(COOH)}$ as shown in Figures 3B and 3C is due to the introduction of an electron transfer (ET) pathway photogenerated from NR to catalyst. The change in PL lifetime can be used to calculate the rate of electron transfer ($k_{ET}$). The $k_{ET}$ was found to increase with concentration due to the increase in surface coverage at higher $M_{bpy(COOH)}$ per NR, as expected from the cumulative kinetics of ET events. Kinetic modeling at trap state and band gap provided the rate constants to be on the orders of $10^7$ $s^{-1}$ and $10^8$ $s^{-1}$, respectively (Details in SI Methods, Table S1). This is in agreement with the timescales of analogous nanoparticle-integrated systems that have been reported.[19,27,28]

The scheme depicted in Figure 4A provides a structural model for the surface coordination formed between $M_{bpy(COOH)}$ and ligand capped CdS NRs discussed above and provides insight into a plausible reaction mechanism involved in 1,4-NADH photogeneration. (Some possibilities of orientation that the Rh-centered catalyst may assume as it coordinates to the surface is also shown guided by the Ru-polypyridine complexes attached to CdSe nanocrystals studied via carboxylate linkages.[40])

Photon absorption by CdS upon light irradiation leads to the generation of electron−hole pairs, facilitating catalysis by the transfer of conduction band electrons to the surface-tethered mediator led by the electron donation to the valence band holes through the oxidation of TEOA. Subsequently, the regiospecific transfer of hydride ions from the reduced form of $M_{bpy(COOH)}$ to the C4 position of $NAD^+$ leads to the production of enzymatically active 1,4-NADH.

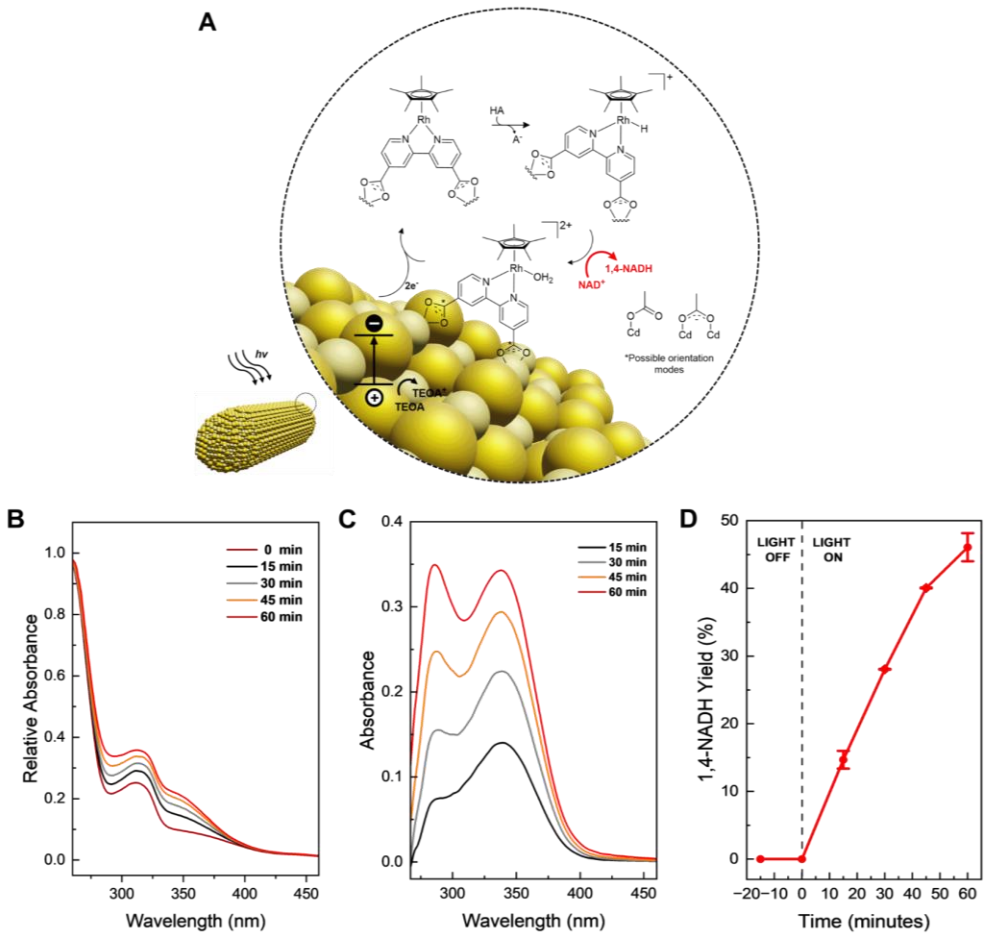


**Figure 4.** (A) Overall schematic of the photogeneration of 1,4-NADH from $NAD^+$ with surface tethered CdS NRs as a light absorber. (B) Changes in UV-vis spectra for a period of 1 hr under photocatalytic conditions. (C) Spectral differences of the absorbance profiles under light irradiation with reaction time using 48 nM CdS NR and 1 mM $NAD^+$. (D) Temporal evolution of 1,4-NADH yield as a percentile with reaction time obtained from quantitative $^1$H-NMR spectroscopy.

The photochemical generation reactions of surface decorated CdS NRs were performed under blue light irradiation ($\lambda$ = 455 nm) at an intensity of 100 mW $cm^{-2}$ in a quartz reactor under inert conditions provided by a continuous flow of argon, with steady stirring, and at room temperature. The reactions were performed to assess the generation of 1 mM $NAD^+$ in a phosphate buffered solution of 0.5 mM at pH 7.3. The progress of the reaction was monitored over one hour, with aliquots withdrawn at 15-minute intervals (Refer SI for further details). Figure 4B illustrates the temporal evolution of absorbance and Figure 4C shows the individual spectral change with respect to the reaction absorption profile at 0 minutes, providing insights into the kinetics and overall progress of the reaction. Although UV-vis spectroscopy is a widely utilized method, its reliability in product quantification is undermined by potential isomer formations during $NAD^+$ reduction (Figure S10). This arises from similarities in absorbance profiles, particularly between 1,4-NADH (at 340 nm), 1,6-NADH (at 345 nm), and $NAD_2$ dimers (~340 nm).[41] This is evident in our control experiments with bare CdS NRs that produces an unstable dimer species (Figure S11). Therefore, to augment the reliability of the collected data, we conducted $^1$H-NMR spectroscopic measurements at each sampling interval to quantify 1,4-NADH (Figure S13). Additionally, enzymatic assays and PL spectroscopy were also employed to corroborate product formation (Figures S15, S16). The calculated efficiencies as a percentile are presented in Figure 4D. As illustrated in Figures 4B to 4D, the formation of 1,4-NADH increases steadily over the reaction time, reaching a maximum efficiency of approximately 50% within 60 minutes. We drove this reaction further for a maximum period of 2 hours before cofactor production declines (Figure S17). The significance of this maximum efficiency is especially impressive because of the exceptionally low concentration of the CdS NRs we use in this reaction. Figures 4B to 4D represent a reaction that was performed using 48 nM of CdS NRs (CdS: $M_{bpy(COOH)}$ 1:11) calculated using its

absorbance at 350 nm as previously mentioned. Therefore, while many report such efficiencies with significantly larger concentrations of nanoparticles or longer reaction times,[16,18,41] we demonstrate that lower NR concentrations can drive the generation of 1,4-NADH to half its maximum capacity in just under an hour. The performance of cofactor generation can be measured by turnover frequency (TOF; the number of moles of 1,4-NADH formed per moles of active site per unit of time), which was found to be 175 $h^{-1}$ which to the best of our knowledge is the uppermost number reported to date for photosensitizer / regiospecific mediator driven 1,4-NADH generation. [16,18,23]

Following this observation, we tested the performance of the parent catalyst, M, which remains freely dispersed in solution due to the absence of binding functional groups. The overall efficiency of 1,4-NADH formed is higher with M (Figure S18), which can be attributed mainly due to the electron-withdrawing nature of the carboxylate groups of $M_{bpy(COOH)}$ which diminishes the basicity of the bipyridine moiety, which is known to decelerate the rate-determining step of hydride complex formation.[11] This causes a decrease of the maximum efficiency of the reaction by 34% compared to that of the untethered complex system. This is similar in observation to a surface functionalized Rh-centered catalyst, a more complex analog of $M_{bpy}$ that reports an activity of around an order of magnitude lower than that of the parent mediator attributed to severe diffusion limitations.[16] This observed correlation emphasizes the impact of structural modifications on catalytic efficiency. Moreover, the TOF for this free mediator system was found to be 266 $h^{-1}$. However, together both these systems record the highest TOF values to date for a photochemical generation of 1,4-NADH with homogeneous or heterogeneous inorganic photosensitizers (Table S2). Our approach mainly distinguishes itself by the large light absorption capacity of NRs attributed to their tunable optical properties. Additionally, the individual contributions of the

components in this reaction such as the CdS NRs can be manipulated by changes in light intensities and the quantitative distribution of molecular complexes. Furthermore, we were also able to explore the derivatization of M with functional groups such as $CH_3$, $OCH_3$, $COOCH_3$; however, the isomers' specificity was poor due to increasing steric effects (Figure S19).

As previously mentioned, we observed a decline in 1,4-NADH production upon prolonged illumination, prompting us to investigate this phenomenon further. NADH and its analogs are known to be unstable in both acidic and neutral buffered solutions. The primary acidic degradation product forms through a hydration step and an acyclization reaction, resulting in NADHX, which absorbs between 285 nm and 300 nm.[42] As shown in Figures 4B and 4C, the increase in the 285 nm region over time, along with evidence presented in Figure S13, supports the conclusion that NADHX is formed. Previous studies have shown that prolonged illumination of Cd-chalcogenide nanocrystals depletes surface thiol ligands, deactivating catalyst performance. [43,44] We explored this by periodically introducing ligand injections equal to less than 0.1% of 3-MPA on the NR. The resulting changes in degradation and 1,4-NADH levels (Figure S20) confirm that the accumulation of mercaptopropionic species increases degradation rates beyond 1,4-NADH production after prolonged illumination ($\geq$ 2 hours). This suggests that 3-MPA accumulation may exceed buffer capacity. To address this, we increased buffer concentration, which, while not completely preventing degradation, significantly mitigates it, as shown in Figure S21. This highlights the need to enhance buffer capacity in systems involving ligand-capped nanoparticles for 1,4-NADH generation.

In addition, we also ruled out degradation of the CdS NRs contributing to the decline in photocatalytic rates as there was no evidence of significant changes in the dimensions based on TEM images or in the UV−vis absorbance profile (Figures S22 and S23 respectively).

Consequently, this study provides a highly efficient model framework for advancing catalyst enhancements for a heterogeneous catalysis approach in 1,4-NADH generation by combining a photosensitizer with a large absorption efficiency and an appropriate band gap with a co-catalytic reaction center tethered to the nanoparticulate assembly, this model facilitates easier product isolation. Unlike free mediator systems, where isolation can be challenging, the attached system simplifies the process, leading to cleaner and more efficient experimental procedures. This advancement supports cleaner and more efficient experimental processes for subsequent studies and spectroscopy probing that include semiconductor mediated photochemical generation of biological cofactors.

ASSOCIATED CONTENT

**Supporting Information**

CdS NR synthesis and band gap measurements, CV, XPS survey scan, FT-IR, UV−vis absorption spectra, τ and $k_{ET}$ calculations, TEM images and distribution of lengths and diameters, synthesis of catalysts and characterization, calculation of extinction coefficients, 2D DOSY experimentation details, isomers of NADH, $^{1}$H-NMR used for 1,4-NADH quantification, quantification of $M_{bpy(COOH)}$ coverage on NRs, bare CdS experiments, derivatization of Rh-based catalyst with $CH_3$, $OCH_3$ and $COOCH_3$, enzymatic assay, buffer capacity changes, Stern-Volmer and Langmuir fits, stability tests, details of 1,4-NADH degradation. (PDF).

AUTHOR INFORMATION

**Corresponding Author**

*E-mail p_yang@berkeley.edu (P.Y.).

## Author Contributions

The manuscript was written through contributions of all authors. All authors have given approval to the definitive version of the manuscript.


## Funding Sources

This work was supported by the NSF under grant DMR-2217161.


## Notes

The authors declare no competing financial interest.


ACKNOWLEDGMENT

We thank Drs. Hasan Celik, Raynald Giovine, and Pines Magnetic Resonance Center's Core NMR Facility (PMRC Core) for spectroscopic assistance. The instruments used in this work are supported by NIH S10OD024998 (AV-600) and the National Science Foundation under Grant No. 2018784 (NEO-400). We would also like to thank Julian Feijóo and Cheng Zhu for assisting with electrochemistry measurements. XPS was performed with assistance and initial training received by Dr. Juliet Jamtgaard at the Stanford Nano Shared Facilities (SNSF, RRID:SCR_023230), supported by the National Science Foundation (ECCS-2026822). J.W. acknowledges fellowship support from Stephen J. Blumenkranz Undergraduate Summer Fellowship.


REFERENCES


(1) Sakimoto, K. K.; Wong, A. B.; Yang, P. Self-Photosensitization of Nonphotosynthetic Bacteria for Solar-to-Chemical Production. *Science* **2016**, *351* (6268), 74–77.

(2) Liu, C.; Gallagher, J. J.; Sakimoto, K. K.; Nichols, E. M.; Chang, C. J.; Chang, M. C. Y.; Yang, P. Nanowire-Bacteria Hybrids for Unassisted Solar Carbon Dioxide Fixation to Value-Added Chemicals. *Nano Lett* **2015**, *15* (5), 3634–3639. .

(3) Zhang, H.; Liu, H.; Tian, Z.; Lu, D.; Yu, Y.; Cestellos-Blanco, S.; Sakimoto, K. K.; Yang, P. Bacteria Photosensitized by Intracellular Gold Nanoclusters for Solar Fuel Production. *Nature Nanotech* **2018**, *13* (10), 900–905.

(4) Kornienko, N.; Sakimoto, K. K.; Herlihy, D. M.; Nguyen, S. C.; Alivisatos, A. P.; Harris, C. B.; Schwartzberg, A.; Yang, P. Spectroscopic Elucidation of Energy Transfer in Hybrid Inorganic-Biological Organisms for Solar-to-Chemical Production. *PNAS* **2016**, *113* (42), 11750–11755.

(5) Kornienko, N.; Zhang, J. Z.; Sakimoto, K. K.; Yang, P.; Reisner, E. Interfacing Nature's Catalytic Machinery with Synthetic Materials for Semi-Artificial Photosynthesis. *Nature Nanotech*. **2018**, *13*, 890–899.

(6) Yang, P.; Cai, R.; Kim, J. M.; Cestellos-Blanco, S.; Jin, J. Microbes 2.0: Engineering Microbes with Nanomaterials. *AsiaChem Magazine* **2020**, *1* (1), 36-41.

(7) Lineberry, E.; Kim, J.; Kim, J.; Roh, I.; Lin, J. A.; Yang, P. High-Photovoltage Silicon Nanowire for Biological Cofactor Production. *J Am Chem Soc* **2023**, *145* (36), 19508–19512.

(8) Shaked, Z; Whitesides, G. M. Enzyme-Catalyzed Organic Synthesis: NADH Regeneration Using Formate Dehydrogenase. *J Am Chem Soc* **1980**, 102, 7104-7105.

(9) Chenault, H. K.; Whitesides, G. M. Lactate Dehydrogenase-Catalyzed Regeneration of NAD from NADH for Use in Enzyme-Catalyzed Synthesis. *Bioinorganic Chemistry* **1989**, 17 (4), 400-409.

(10) Wagenknecht, P. S.; Penney, J. M.; Hembre, R. T. Transition-Metal-Catalyzed Regeneration of Nicotinamide Coenzymes with Hydrogen. *Organometallics* **2003**, *22* (6), 1180–1182.

(11) Walcarius, A.; Nasraoui, R.; Wang, Z.; Qu, F.; Urbanova, V.; Etienne, M.; Göllü, M.; Demir, A. S.; Gajdzik, J.; Hempelmann, R. Factors Affecting the Electrochemical Regeneration of NADH by (2,2'-Bipyridyl) (Pentamethylcyclopentadienyl)-Rhodium Complexes: Impact on Their Immobilization onto Electrode Surfaces. *Bioelectrochemistry* **2011**, *82* (1), 46–54.

(12) Wienkamp, R.; Steckhan, E. Indirect Electrochemical Regeneration of NADH by a Bipyridinerhodium(I) Complex as Electron-Transfer Agent. *Angewandte Chemie International Edition in English* **1982**, *21* (10), 782–783.

(13) Singh, A.; Yadav, R. K.; Yadav, U.; Kim, T. W. Highly Efficient Flower-Like Graphene Quantum Dots-Based Fuschin Photocatalyst for Selective NAD(P)H Cofactor Regeneration Under Solar Light Irradiation. *Photochem Photobiol* **2022**, *98* (2), 412–420.

(14) Wu, H.; Tian, C.; Song, X.; Liu, C.; Yang, D.; Jiang, Z. Methods for the Regeneration of Nicotinamide Coenzymes. *Green Chemistry* **2013**, 15 (7), 1773–1789.

(15) Tensi, L.; Macchioni, A. Extremely Fast NADH-Regeneration Using Phosphonic Acid as Hydride Source and Iridium-Pyridine-2-Sulfonamidate Catalysts. *ACS Catal* **2020**, *10* (14), 7945–7949.

(16) De Torres, M.; Dimroth, J.; Arends, I. W. C. E.; Keilitz, J.; Hollmann, F. Towards Recyclable NAD(P)H Regeneration Catalysts. *Molecules* **2012**, *17* (8), 9835–9841.

(17) Ganesan, V.; Sivanesan, D.; Yoon, S. Correlation between the Structure and Catalytic Activity of [Cp*Rh(Substituted Bipyridine)] Complexes for NADH Regeneration. *Inorg Chem* **2017**, *56* (3), 1366–1374.

(18) Nam, D. H.; Lee, S. H.; Park, C. B. CdTe, CdSe, and CdS Nanocrystals for Highly Efficient Regeneration of Nicotinamide Cofactor under Visible Light. *Small* **2010**, *6* (8), 922–926.

(19) Utterback, J. K.; Ruzicka, J. L.; Keller, H. R.; Pellows, L. M.; Dukovic, G. Electron Transfer from Semiconductor Nanocrystals to Redox Enzymes. *Annu Rev Phys Chem* **2020**, *71*, 335-359.

(20) Shulenberger, K. E.; Jilek, M. R.; Sherman, S. J.; Hohman, B. T.; Dukovic, G. Electronic Structure and Excited State Dynamics of Cadmium Chalcogenide Nanorods. *Chemical Reviews*. **2023**, *123* (7), 3852–3903.

(21) Kamal, J. S.; Gomes, R.; Hens, Z.; Karvar, M.; Neyts, K.; Compernolle, S.; Vanhaecke, F. Direct Determination of Absorption Anisotropy in Colloidal Quantum Rods. *Phys Rev B Condens Matter Mater Phys* **2012**, *85* (3), 035126-1-7.

(22) Zhu, H.; Lian, T. Enhanced Multiple Exciton Dissociation from CdSe Quantum Rods: The Effect of Nanocrystal Shape. *J Am Chem Soc* **2012**, *134* (27), 11289–11297.

(23) Ruppert, R.; Herrmann, S.; Steckhan, E. Very Efficient Reduction of $NAD(P)^+$ with Formate Catalysed by Cationic Rhodium Complexes, *J. Chem. Soc., Chem. Commun.*, **1988**, (17), 1150-1151.

(24) Sykora, M.; Petruska, M. A.; Alstrum-Acevedo, J.; Bezel, I.; Meyer, T. J.; Klimov, V. I. Photoinduced Charge Transfer between CdSe Nanocrystal Quantum Dots and Ru-Polypyridine Complexes. *J Am Chem Soc* **2006**, *128* (31), 9984–9985.

(25) Robinson, R. D.; Sadtler, B.; Demchenko, D. O. E.; Can K. Wang, L.-W.; Alivisatos, A. P. Spontaneous Superlattice in Nanorods Through Partial Cation Exchange. *Science* **2007**, *317* (5836), 355–358.

(26) Todorova, T. K.; Huan, T. N.; Wang, X.; Agarwala, H.; Fontecave, M. Controlling Hydrogen Evolution during Photoreduction of $CO_2$ to Formic Acid Using $[Rh(R\text{-}Bpy)(Cp^*)Cl]^+$ Catalysts: A Structure-Activity Study. *Inorg Chem* **2019**, *58* (10), 6893–6903.

(27) Wolff, C. M.; Frischmann, P. D.; Schulze, M.; Bohn, B. J.; Wein, R.; Livadas, P.; Carlson, M. T.; Jäckel, F.; Feldmann, J.; Würthner, F.; Stolarczyk, J. K. All-in-One Visible-Light-Driven Water Splitting by Combining Nanoparticulate and Molecular Co-Catalysts on CdS Nanorods. *Nat Energy* **2018**, *3* (10), 862–869.

(28) Tseng, H. W.; Wilker, M. B.; Damrauer, N. H.; Dukovic, G. Charge Transfer Dynamics between Photoexcited CdS Nanorods and Mononuclear Ru Water-Oxidation Catalysts. *J Am Chem Soc* **2013**, *135* (9), 3383–3386.

(29) Ryu, J.; Nam, D. H.; Lee, S. H.; Park, C. B. Biocatalytic Photosynthesis with Water as an Electron Donor. *Chemistry - A European Journal* **2014**, *20* (38), 12020–12025.

(30) Sachleben, J. R.; Wrenn Wooten, E.; Emsley, L.; Pines, A.; Colvin, V. L.; Alivisatos, A. P. NMR Studies of the Surface Structure and Dynamics of Semiconductor Nanocrystals. *Chemical Physics Letters* **1992**, *198* (5), 431-436.

(31) Ji, X.; Copenhaver, D.; Sichmeller, C.; Peng, X. Ligand Bonding and Dynamics on Colloidal Nanocrystals at Room Temperature: The Case of Alkylamines on CdSe Nanocrystals. *J Am Chem Soc* **2008**, *130* (17), 5726–5735.

(32) Holland, G. P.; Sharma, R.; Agola, J. O.; Amin, S.; Solomon, V. C.; Singh, P.; Buttry, D. A.; Yarger, J. L. NMR Characterization of Phosphonic Acid Capped $SnO_2$ Nanoparticles. *Chemistry of Materials* **2007**, *19* (10), 2519–2526.

(33) Tavasoli, E.; Guo, Y.; Kunal, P.; Grajeda, J.; Gerber, A.; Vela, J. Surface Doping Quantum Dots with Chemically Active Native Ligands: Controlling Valence without Ligand Exchange. *Chemistry of Materials* **2012**, *24* (21), 4231–4241.

(34) Dhaene, E.; Billet, J.; Bennett, E.; Van Driessche, I.; De Roo, J. The Trouble with ODE: Polymerization during Nanocrystal Synthesis. *Nano Lett* **2019**, *19* (10), 7411–7417.

(35) Hens, Z.; Martins, J. C. A Solution NMR Toolbox for Characterizing the Surface Chemistry of Colloidal Nanocrystals. *Chemistry of Materials* **2013**, *25* (8), 1211–1221.

(36) Munro, A. M.; Plante, I. J. La; Ng, M. S.; Ginger, D. S. Quantitative Study of the Effects of Surface Ligand Concentration on CdSe Nanocrystal Photoluminescence. *Journal of Physical Chemistry C* **2007**, *111* (17), 6220–6227.

(37) Brown, K. A.; Song, Q.; Mulder, D. W.; King, P. W. Diameter Dependent Electron Transfer Kinetics in Semiconductor-Enzyme Complexes. *ACS Nano* **2014**, *8* (10), 10790–10798.

(38) Jones, M.; Scholes, G. D. On the Use of Time-Resolved Photoluminescence as a Probe of Nanocrystal Photoexcitation Dynamics. *J Mater Chem* **2010**, *20* (18), 3533–3538.

(39) Brumberg, A.; Diroll, B. T.; Nedelcu, G.; Sykes, M. E.; Liu, Y.; Harvey, S. M.; Wasielewski, M. R.; Kovalenko, M. V.; Schaller, R. D. Material Dimensionality Effects on Electron Transfer Rates between $CsPbBr_3$ and CdSe Nanoparticles. *Nano Lett* **2018**, *18* (8), 4771–4776.

(40) Koposov, A. Y.; Cardolaccia, T.; Albert, V.; Badaeva, E.; Kilina, S.; Meyer, T. J.; Tretiak, S.; Sykora, M. Formation of Assemblies Comprising Ru-Polypyridine Complexes and CdSe Nanocrystals Studied by ATR-FTIR Spectroscopy and DFT Modeling. *Langmuir* **2011**, *27* (13), 8377–8383.

(41) Saba, T.; Li, J.; Burnett, J. W. H.; Howe, R. F.; Kechagiopoulos, P. N.; Wang, X. NADH Regeneration: A Case Study of Pt-Catalyzed $NAD^+$ Reduction with $H_2$. *ACS Catal* **2021**, *11* (1), 283–289.

(42) Johnson, S. L.; Tuazon, P. T. Acid-Catalyzed Hydration of Reduced Nicotinamide Adenine Dinucleotide, and Its Analogues. *Biochemistry* **1977**; *16* (6), 1175-83.

(43) Aldana, J.; Wang, Y. A.; Peng, X. Photochemical Instability of CdSe Nanocrystals Coated by Hydrophilic Thiols. *J Am Chem Soc* **2001**, *123* (36), 8844–8850.

(44) Brown, K. A.; Wilker, M. B.; Boehm, M.; Dukovic, G.; King, P. W. Characterization of Photochemical Processes for H 2 Production by CdS Nanorod-[FeFe] Hydrogenase Complexes. *J Am Chem Soc* **2012**, *134* (12), 5627–5636.

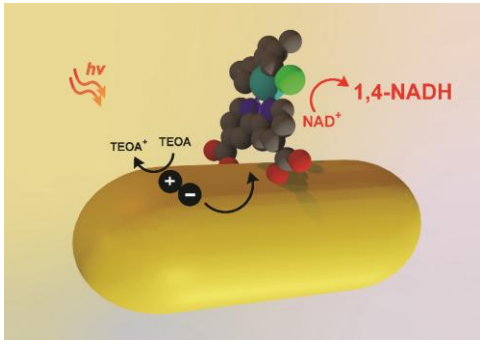


For Table of Contents Only